NANO LETTERS

Letter

pubs.acs.org/NanoLett

Low-Temperature Ohmic Contact to Monolayer MoS_2 by van der Waals Bonded Co/*h*-BN Electrodes

Xu Cui,[†,¶] En-Min Shih,[‡,¶] Luis A. Jauregui,[§] Sang Hoon Chae,[†] Young Duck Kim,[†,∥] Baichang Li,[†] Dongjea Seo,[⊥] Kateryna Pistunova,[§] Jun Yin,[#] Ji-Hoon Park,[∇,○] Heon-Jin Choi,[⊥] Young Hee Lee,[∇,○] Kenji Watanabe,[◆] Takashi Taniguchi,[◆] Philip Kim,[§] Cory R. Dean,[*,‡] and James C. Hone[*,†]

[†]Department of Mechanical Engineering and [‡]Department of Physics, Columbia University, New York, New York 10027, United States

[§]Department of Physics, Harvard University, Cambridge, Massachusetts 02138, United States

[∥]Department of Physics and Center for Humanities and Sciences, Kyung Hee University, Seoul 02447, Republic of Korea

[⊥]Department of Materials Science and Engineering, Yonsei University, 120-749 Seoul, Republic of Korea

[#]State Key Laboratory of Mechanics and Control of Mechanical Structures, Institute of Nanoscience, Nanjing University of Aeronautics and Astronautics, Nanjing 210016, China

[∇]Center for Integrated Nanostructure Physics, Institute for Basic Science (IBS), Suwon 16419, Republic of Korea

[○]Department of Energy Science, Sungkyunkwan University (SKKU), Suwon 16419, Republic of Korea

[◆]National Institute for Materials Science, 1-1 Namiki, Tsukuba 305-0044, Japan

Supporting Information

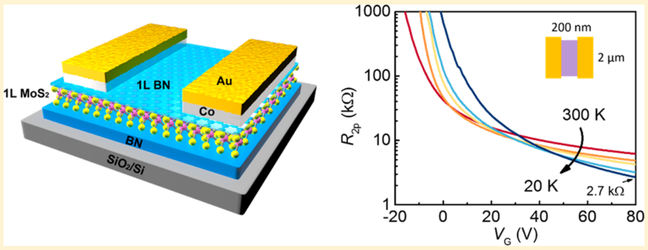

ABSTRACT: Monolayer MoS_2, among many other transition metal dichalcogenides, holds great promise for future applications in nanoelectronics and optoelectronics due to its ultrathin nature, flexibility, sizable band gap, and unique spin-valley coupled physics. However, careful study of these properties at low temperature has been hindered by an inability to achieve low-temperature Ohmic contacts to monolayer MoS_2, particularly at low carrier densities. In this work, we report a new contact scheme that utilizes cobalt (Co) with a monolayer of hexagonal boron nitride (h-BN) that has the following two functions: modifies the work function of Co and acts as a tunneling barrier. We measure a flat-band Schottky barrier of 16 meV, which makes thin tunnel barriers upon doping the channels, and thus achieve low-T contact resistance of 3 k$\Omega.\mu$m at a carrier density of $5.3 \times 10^{12}/\text{cm}^2$. This further allows us to observe Shubnikov–de Haas oscillations in monolayer MoS_2 at much lower carrier densities compared to previous work.

KEYWORDS: *Work-function, tunneling contact, monolayer MoS_2, low temperature*

Transition-metal dichalcogenides (TMDCs), which can be isolated as single monolayers either by exfoliation from bulk crystals or by direct synthesis, have attracted widespread recent interest due to their unique properties and potential for applications.[1−6] Among those, MoS_2 is the most widely studied. In the monolayer limit, it is a direct-gap semiconductor[2] and hosts fascinating physical behavior near the band edge at the K-point, including valley-spin coupled physics[7] that gives rise to a variety of phenomena including the valley Hall effect.[3] However, its large bandgap (2.15 eV measured by scanning tunneling spectroscopy) of monolayer MoS_2[8] (as well as that of similar materials such as $MoSe_2$, WS_2, and WSe_2) makes achieving Ohmic electrical contacts highly challenging, and in fact the contact problem has been highlighted as a central challenge for both applications and basic studies.[9,10] A great deal of recent experimental work has demonstrated progress toward improved contacts. This includes use of low-work function metals,[11,12] graphene,[13−15] or doped TMDCs[16] as electrodes, thermal annealing,[17] ionic-liquid doping of the contact regions,[18,19] phase-engineering,[20] selective etching,[21,22] and introduction of thin tunnel barriers.[23−25] However, this work has largely focused on few layer TMDCs and room-temperature behavior (see in Supporting Information S1). Low-temperature contact to monolayer TMDCs remains a significant challenge.

In this study, we focus on the challenge of obtaining low-resistance contacts to the conduction band of monolayer MoS_2 at low temperature. This is a critical prerequisite for detailed study of quantum transport,[26] valley-tronic properties,[27] and transport signatures of interlayer excitonic states.[28,29] We have previously demonstrated that few-layer graphene can achieve

Received: April 12, 2017
Revised: July 6, 2017
Published: July 10, 2017

DOI: 10.1021/acs.nanolett.7b01536
Nano Lett. 2017, 17, 4781−4786

robust low-T contact to few-layer MoS_2 at moderate carrier densities,[13] but reliable contact to monolayer MoS_2 is only achieved at high carrier densities ($\sim 1 \times 10^{13}$ /cm^2), making phenomena near the band edge inaccessible. Similar results have been seen for Au contacts, where low contact resistance is achieved only after aggressive thermal annealing, which can negatively affect the channel characteristics due to the creation of sulfur vacancies.[17] Low work-function metals such as Sc and Al have also been explored and perform well at room temperature but show non-Ohmic contact behavior at low temperature (Supporting Information S2).[11,12]

Recently, Farmanbar et al. proposed a new route to achieve stable low work function metal contacts to TMDs.[30,31] In this scheme, a monolayer of graphene or h-BN is placed between a transition metal contact and the TMDC. The monolayer spacer serves two advantageous purposes: it strongly interacts with the transition metal, reducing its work function by over 1 eV, and it breaks the metal−TMDC interaction to eliminate the interface states that cause Fermi level pinning. Here, we experimentally validate this prediction. We use cobalt electrodes with monolayer h-BN to achieve substantially improved low-T contacts to monolayer MoS_2 and verify the work function modification directly using X-ray photoemission spectroscopy. Multiterminal magneto-transport measurements show that Ohmic contacts are achieved at low carrier density of 3.5×10^{12} cm^{-2}, allowing Hall mobility measurement and the observation of quantum oscillations to lower carrier densities than previously possible.

Figure 1a shows a schematic of the devices used in this study. MoS_2 and h-BN were exfoliated from bulk crystals (MoS_2 obtained from SPI Supplies) onto SiO_2 (285 nm)/Si substrates and identified by optical microscopy with thickness verified by Raman spectroscopy, photoluminescence, and atomic force microscopy (Supporting Information S3). Next, following the previously described dry van der Waals transfer method,[32] a polymer film was used pick up a stack of ~30 nm thick h-BN (top), 1L MoS_2 (middle), and 1L h-BN (bottom). The polymer and stack were inverted and placed, polymer down, on a Si/SiO_2 substrate, and then heated in vacuum at 250 C for 30 min to remove the supporting polymer (Supporting Information S4 for details). We verify below that this process does not introduce any extra doping. Subsequently, the stack was patterned into the desired shape by e-beam lithography followed by SF_6/O_2 plasma etching. Finally, 30 nm Co and 50 nm Au electrodes were patterned by a second e-beam lithography step, electron beam evaporation, and liftoff. For the devices described below (unless noted otherwise), we evaporated Co under ultrahigh vacuum (UHV) conditions ($\sim 10^{-10}$ Torr) to minimize interfacial contamination and Co oxidation. We find that this method produces the lowest contact resistance and highest yield, as described below. We also found similar results using chemical vapor deposition (CVD)-grown monolayer h-BN on CVD monolayer MoS_2 (Supporting Information S5), confirming the possibility of large-scale applications.

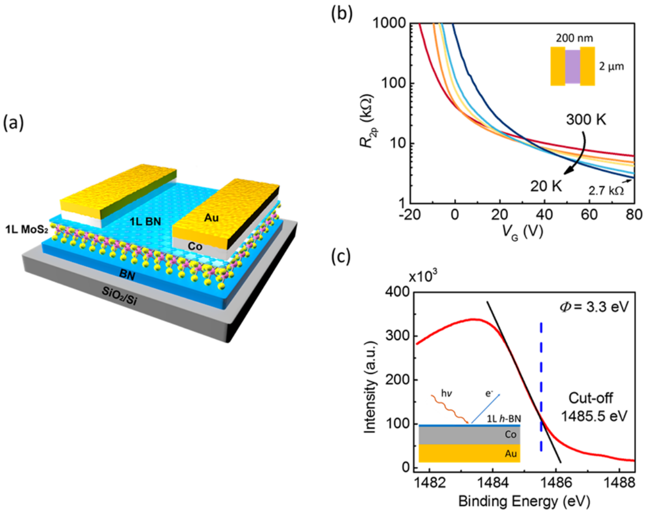

Figure 1. Device geometry, two-probe transport measurement, and work function measurement. (a) Device schematic for Co/h-BN/1L MoS_2 contact. (b) Two-probe measurement for a short channel device with 2 μm width and 200 nm length. The minimum resistance at 20 K is 2.7 kΩ·μm that sets the upper-bound limit for the contact resistance. (c) Inelastic second cutoff. XPS spectrum of cobalt film covered by single layer CVD h-BN using Thermo Scientific K-Alpha ($h\nu$ = 1486.6 eV) with −30 V bias. The work-function is determined by the energy difference between the cutoff and Fermi edge (see Supporting Information, Figure S10) subtracted from the source energy ($h\nu$ = 1486.6 eV), thus h-BN/Co work-function (Φ) = 3.3 eV.

As a first demonstration, we examine the quality of the contacts by performing gate-dependent transport measurements on a short channel (200 nm) two-terminal device, at temperatures from 20 to 300 K (Figure 1b). Characteristic of an n-type FET, the two-terminal resistance decreases with increasing gate voltage. Above ~30 V, the resistance decreases with decreasing temperature, indicative of metallic conduction in the channel and barrier-free contacts, and falls below 2.7 kΩ·μm at V_g = 80 V and T = 20 K. Furthermore, at all temperatures the resistance is lower than 100 kΩ·μm for gate voltages larger than 10 V. This provides strong initial evidence that the proposed technique does indeed provide good contacts.

We next confirmed the low work-function of h-BN/Co using XPS on a large-area Co/h-BN film. This sample was created by evaporating 30 nm of Co onto CVD-grown h-BN transferred onto a Si/SiO_2 wafer, then peeling the film from the substrate and inverting it. In this way, a pristine Co/h-BN interface could be studied without oxidation of the Co. The XPS spectrum was measured using a Thermo Scientific K-Alpha XPS system ($h\nu$ = 1486.6 eV), using an applied stage bias of −30 V, so the cutoff of the sample can be distinguished (cutoff energy = 1485.5 eV, as shown in Figure 1c). The spectrum width is determined by the difference between the cutoff energy and the Fermi edge (spectrum width = 1483.3 eV). The Fermi edge position is determined by the center of the first rising slope, while the cutoff energy is determined by the change of slope (maximum of the second derivative, Supporting Information S6). The work function (Φ) of the film is determined by subtracting the spectrum width from the Al Kα line (1486.6 eV), resulting in Φ = 3.3 eV,[33] which is 1.7 eV smaller than Co work-function of 5.0 eV.[34] We also checked the work function of a thick Au film (after 5 min of in situ Ar ion milling to remove any contamination on the surface) and obtained Φ = 5.2 eV, which is in good agreement with published values.

Having established that the Co/h-BN structure has a low work function and provides very good contacts to MoS_2, we studied the properties of these contacts in more detail using multiterminal devices in a Hall bar geometry (Figure 2a), which allows independent determination of the channel resistance, contact resistance, and carrier density. First, we performed two-

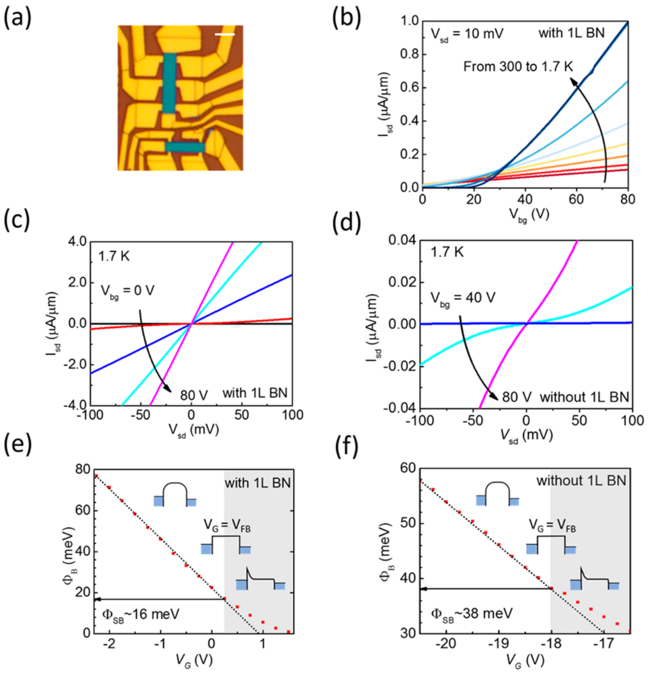

Figure 2. Hall bar geometry devices images, transfer curves, *I*−*V* curves and Schottky barrier measurements. (a) Optical image of a Co/1L h-BN/1L MoS_2 contact device. Scale bar is 2 μm. (b) Two-terminal source-drain current, I_{sd}, of the Co/1L h-BN/1L MoS_2 contact device as a function of back-gate voltage, V_{bg}. Temperature from 300 to 1.7 K are denoted with traces colored from red to blue. The dc source-drain voltage, V_{sd}, was 10 mV. (c) Low-bias output characteristics of Co/1L h-BN contact showing linear I_{sd}−V_{sd} behavior starts at the turn-on gate voltage (20 V), indicating the Ohmic nature even at 1.7 K. (d) Low-bias output characteristics of Co direct contact to 1L MoS_2 showing nonlinear I_{sd}−V_{sd} behavior, indicating non-Ohmic behavior at 1.7 K. (e,f) Schottky barrier measurement with activation energy method. The activation energy, Φ_B, is extracted from the slope of an Arrhenius plot (Supporting Information S9). The Schottky barrier height is the activation energy at the flat-band gate voltage. For (e) 1L h-BN/Co contact the Schottky barrier is ∼16 meV, whereas for (f) Co direct contact it is ∼38 meV.

probe direct current (dc) measurements between the source and drain of the Hall bar, at temperatures from room temperature to 1.7 K. The low-bias transfer curve (Figure 2b) shows consistent behavior with the short-channel device (Figure 1b); above a gate voltage of 25 V, the current increases with decreasing temperature, indicating that transport is metallic rather than activated. The output curves (current vs bias voltage) are linear at gate voltages above 0 V at room temperature (Supporting Information S7) and above 20 V at 1.7 K (Figure 2c, Supporting Information S8).

Control experiments allow us to verify the unique dual role of the h-BN in combination with a transition metal contact. First, the contact quality is found to be much poorer for Co without h-BN, for which the output *I*−*V* curves are linear at room *T* (Supporting Information S7), but nonlinear at low *T* (Figure 2d) even at large gate voltage. Such nonlinear behavior is particularly detrimental for the voltage contacts in multi-terminal measurements, which operate in the limit of very low bias. Second, other metals (Sc, Ti, Al, Ag) with 1L h-BN tunnel barriers, do not provide low-*T* Ohmic contact (Supporting Information S2), confirming that the work function tuning provided by the strong h-BN/Co interaction is critical. This is consistent with previous studies of metal-TMD tunneling contacts using MgO, TiO_2, Ta_2O_5, and h-BN as the insertion layer,[23−25,35,36] which showed a decrease in Fermi level pinning but did not achieve Ohmic contact to monolayer TMDCs at cryogenic temperatures.

The barrier-free behavior for the h-BN/Co contacts is further confirmed by extracting the activation energy from the slope of an Arrhenius plot of $\ln(I/T^{1.5})$ versus $1000/T$ (Supporting Information S9). The derived activation energy is plotted as a function of gate voltage for devices with (Figure 2e) and without (Figure 2f) 1L h-BN. In these plots, the Schottky barrier height is the activation energy at the flat-band gate voltage, seen as the point where the activation energy ceases to decrease linearly with gate voltage;[10] this analysis technique has been used to measure barrier heights of 30−200 meV[11,24,25,36,37] for contacts to multilayer MoS_2. (see Supporting Information S9 for detailed discussion). Using the same technique, we obtain Schottky barrier heights of 16 meV for Co contact with 1L h-BN and 38 meV for Co direct contact to 1L MoS_2 (Figure 2f). We note two important limitations of this analysis. First, the measured value of 16 meV is close to the disorder limit of our sample (Supporting Information S10). Second, it does not account for the presence of the 1L h-BN tunnel barrier, which should act in series with the Schottky barrier.[38−40] Therefore, more detailed modeling will be required for precise quantification of the barrier height. Nevertheless, the above analysis clearly indicates both that the h-BN/Co is an improvement over both Co alone and previous reports.

Next, two-probe and four-probe resistance measurements were combined with Hall effect measurements to determine the channel resistivity and contact resistance as a function of carrier density. Measurements were performed using alternating current (ac) bias (100 nA) with simultaneous lock-in measurement of two-probe (V_{2p}) and four-probe voltage drops (V_{4p}) (Figure 3a inset). We calculated the channel resistivity as $\rho_{xx} = V_{4p}/I_{sd} \times W/L_{4p}$, and the contact resistance

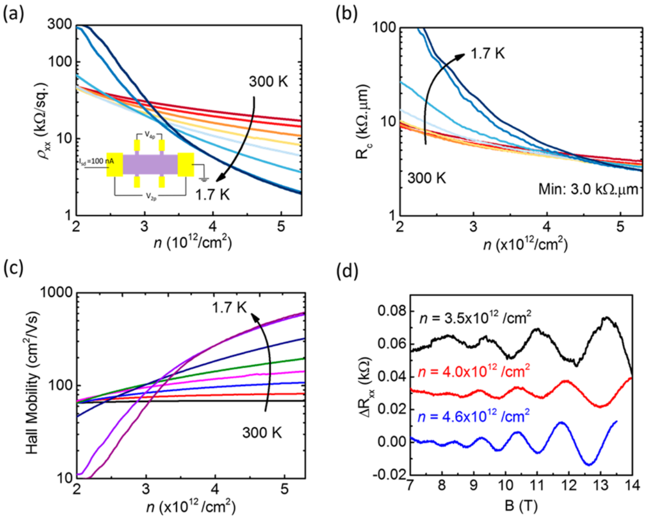

Figure 3. Channel resistivity, contact resistance as a function of temperature, carrier density, and magnetic field. Four-probe resistivity (a), contact resistance (b), and Hall mobility (c) as a function of carrier density at temperatures of 300, 250, 200, 150, 100, 50, 10, and 1.7 K. (d) Shubnikov−de Haas oscillations of monolayer MoS_2 at different carrier densities of 3.5 × 10^{12}/cm^2, 4 × 10^{12}/cm^2, and 4.6 × 10^{12}/cm^2 at T = 1.7 K.

DOI: 10.1021/acs.nanolett.7b01536
Nano Lett. 2017, 17, 4781−4786

as $R_c = (V_{2p}/I_{sd} - (V_{4p}/I_{sd}) \times L_{2p}/L_{4p}) \times W$, where I_{sd} is the source-drain current, L_{2p} is the length between the source and drain contacts, L_{4p} is the length between the voltage contacts, and W is the channel width. The carrier density n was determined by measuring Hall voltage under an applied magnetic field (Supporting Information S11). We find that that the conduction band edge ($n = 0$) is close to 0 V (±3 V), indicating that our samples are not heavily doped during the fabrication process, and that the carrier density obtained from Hall measurements agrees well with the predicted value from the gate capacitance.

Figure 3a,b shows the derived channel resistivity and contact resistance for a typical device (all three measured devices show similar behavior), as a function of carrier density at temperatures from 300 to 1.7 K. Importantly, we find that the robust h-BN/Co contact allows us to reliably measure multiterminal transport for densities down to 2×10^{12} /cm^2. The resistivity (Figure 3a) decreases with increasing carrier density and shows a crossover from nonmetallic to metallic temperature dependence near 3×10^{12} /cm^2. We note that prior work reported a similar crossover but at roughly twice the density, emphasizing the role of disorder in this transition.[17,41] This is attributed to bottom h-BN on SiO$_2$ by the reduced trap density.[42] The contact resistance is strongly dependent on carrier density and temperature. At room temperature, the contact resistance decreases from 10 kΩ·μm at $n = 2 \times 10^{12}$/cm^2 to 4 kΩ·μm at $n = 5 \times 10^{12}$/cm^2, whereas at base temperature (1.7 K), the contact resistance decreases from 100 to 3.0 kΩ·μm over the same density range. The contact resistance decreases with temperature when the carrier density is above ∼4−4.5 × 10^{12}/cm^2, indicating true Ohmic contact behavior at a significantly lower density than previously achieved.

Figure 3c shows the derived Hall mobility for n ranging from 2−5.3 × 10^{12}/cm^2. We note that the behavior of this device is not expected to reflect the intrinsic behavior of MoS$_2$ in the clean limit, because the 1L h-BN top encapsulation layer may not be sufficient to screen external charge disorder, for example, from PMMA resist residue; instead, this serves as a demonstration of the wider density range accessible using the h-BN/Co contacts. The derived Hall mobility $\mu = 1/ne\rho$ (Supporting Information S12) shows phonon limited mobility above 100 K with $\mu_{ph} \sim T^{-\gamma}$. We obtain a value of $\gamma = 0.55$−0.9, much lower than previously observed for a device fully encapsulated by thick h-BN,[13] confirming the presence of extrinsic scattering. The low-temperature mobility reaches ∼630 cm^2/(V s) at carrier density of 5.3×10^{12}/cm^2, comparable to what we have previously observed for CVD-grown monolayer MoS$_2$ at somewhat higher densities (8−10 × 10^{12}/cm^2).[13] Figure 3c also illustrates the disorder-driven crossover to insulating behavior at low density (<4 × 10^{12} cm^2/(V s)) at low temperature (50, 10, 1.7 K), much smaller than the previously reported value of 1−2 × 10^{13} /cm^2.[17,41] Figure 3d shows the longitudinal resistance R_{xx} as a function of applied perpendicular magnetic fields up to 14 T at 1.7 K. We can observe quantum (Shubnikov−de Haas) oscillations at carrier densities down to 3.5×10^{12} /cm^2 and the expected tuning of the oscillation period with gate voltage. Previously, quantum oscillations can be only observed at very high carrier densities around 1×10^{13} /cm^2 for monolayer or moderate carrier density (∼3.7 × 10^{12} /cm^2) for few layers.[13,22] The quantum mobility can be extracted from the onset (∼8 T) of the oscillation: $\mu_q \sim 1/B_q$[43] ∼ 1250 cm^2/(V s). The periodicity of the SdH oscillations can be extracted to estimate the carrier density, or equivalently to measure the level degeneracy g for a known density. For all 1L samples, we observe $2 < g < 4$, indicating that the bands may be partially valley−spin split: the Hall carrier density includes all carrier in the channel whereas the carrier reflected by the periodicity of oscillations tend to pick up the signal from the higher-mobility band and might lead to an underestimate of g factor. This is consistent with previous observations but more detailed study is required to explore this splitting in detail.[44,45]

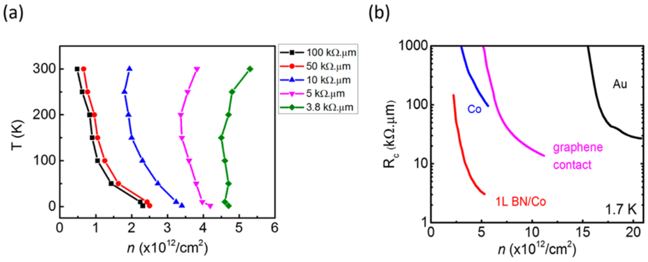

Figure 4. Comparison of monolayer MoS$_2$ contact resistance as a function of temperature and carrier density. (a) Contour plot of contact resistance (100, 50, 10, 5, and 3.8 kΩ.μm, respectively) as a function of temperature and carrier density. (b) Comparison of h-BN tunneling Co contact with different contact schemes in the literatures.[13,17]

Figure 4 summarizes the performance of the h-BN/Co contacts in two different ways. Figure 4a shows contours in temperature and density for R_c = 100, 50, 10, 5, and 3.8 kΩ·μm. Figure 4b shows the low-T contact resistance versus carrier density for the h-BN/Co contacts compared to other methods for monolayer MoS$_2$. First, we note that the contact resistance is roughly 5 times larger when ordinary high vacuum (∼10^{-8} Torr) is used for Co evaporation (Supporting Information S13), which is consistent with improvements seen for UHV evaporation of Au contacts.[46] Elimination of the 1L h-BN (with UHV Co evaporation) also results in a poorer contact. The use of few-layer graphene can provide an adequate contact ($R_c \sim 10$ kΩ·μm) but only at large carrier densities, ∼10^{13}/cm^2.[13] Finally, the previously reported high quality contacts using Au only achieve low resistance for even higher densities, for example, above 2×10^{13} /cm^2.[17] Thus, we conclude that the h-BN/Co structure provides a superior contact to any other reported method and is particularly well suited to studies of properties at low temperature and low carrier density.

In conclusion, we have demonstrated a new contact scheme to the conduction band of monolayer MoS$_2$ that is robust at low temperature and at low carrier density in which monolayer h-BN is inserted between Co and MoS$_2$. This scheme provides the best contacts reported to date, 3.0 kΩ·μm at $n = 5.3 \times 10^{12}$/cm^2 at 1.7 K. Finally, we present the observation of quantum oscillations at carrier density as low as 3.5×10^{12}/cm^2. Further improvement of the quality of the material and channel encapsulation, combined with this contact scheme, will allow us to explore details of quantum transport behavior in the conduction band of large-gap TMDC semiconductors that have remained largely inaccessible. In addition, h-BN/transition contacts may prove useful for electron injection in a wide range of other systems.

■ ASSOCIATED CONTENT

Ⓢ Supporting Information

The Supporting Information is available free of charge on the ACS Publications website at DOI: 10.1021/acs.nanolett.7b01536.

> MoS_2 contact techniques summary; contacts with low work-function metals; Co/h-BN/MoS_2 device fabrication and characterization; device characterization of CVD h-BN and CVD MoS_2; XPS characterization of Co/*h*BN; room-temperature and low-temperature output curve characterization; Schottky barrier extraction; disorder analysis; Hall measurement and Hall mobility; contacts deposited at different pressure (PDF)

■ AUTHOR INFORMATION

Corresponding Authors

*E-mail: jh2228@columbia.edu. Phone (212) 854-6244 (J.C.H).

*E-mail: cd2478@columbia.edu. Phone: (212) 854-3189 (C.R.D.).

ORCID

Xu Cui: 0000-0001-8432-8756

Ji-Hoon Park: 0000-0003-4776-5206

Young Hee Lee: 0000-0001-7403-8157

Author Contributions

¶X.C. and E.-M.S. contributed equally to this work.

Notes

The authors declare no competing financial interest.

■ ACKNOWLEDGMENTS

This research was primarily supported by the NSF MRSEC programme through Columbia in the Center for Precision Assembly of Superstratic and Superatomic Solids (DMR-1420634) and Global Research Laboratory (GRL) Program (2016K1A1A2912707) funded by the Ministry of Science, ICT and Future Planning via the National Research Foundation of Korea (NRF). Low-T magneto transport measurements were supported by the Air Force Office of Scientific Research under Award FA9550-14-1-0268. Work function measurements were supported by the STC Center for Integrated Quantum Materials, NSF Grant DMR-1231319. P.K. and L.A.J. acknowledge Samsung GRP for partial support. J.H.P. and Y.H.L. acknowledge the support by IBS-R011-D1. X.C. and E.M.S acknowledge Professor John Kymissis for discussions regarding the utility of tunnel barrier contacts, and Dr. Rebeca Ribeiro and Dr. Younghun Jung for discussions during the manuscript preparation.

■ REFERENCES

(1) Radisavljevic, B.; Radenovic, A.; Brivio, J.; Giacometti, V.; Kis, A. *Nat. Nanotechnol.* **2011**, *6*, 147−150.

(2) Mak, K. F.; Lee, C.; Hone, J.; Shan, J.; Heinz, T. F. *Phys. Rev. Lett.* **2010**, 136805.

(3) Mak, K. F.; McGill, K. L.; Park, J.; McEuen, P. L. *Science* **2014**, *344*, 1489−1492.

(4) Jones, A. M.; Yu, H.; Ghimire, N. J.; Wu, S.; Aivazian, G.; Ross, J. S.; Zhao, B.; Yan, J.; Mandrus, D. G.; Xiao, D.; Yao, W.; Xu, X. *Nat. Nanotechnol.* **2013**, *8*, 634−638.

(5) Li, X.; Zhang, F.; Niu, Q. *Phys. Rev. Lett.* **2013**, *110*, 066803.

(6) van der Zande, A. M.; Huang, P. Y.; Chenet, D. A.; Berkelbach, T. C.; You, Y.; Lee, G.-H.; Heinz, T. F.; Reichman, D. R.; Muller, D. A.; Hone, J. C. *Nat. Mater.* **2013**, *12*, 554−561.

(7) Xiao, D.; Liu, G.-B.; Feng, W.; Xu, X.; Yao, W. *Phys. Rev. Lett.* **2012**, *108*, 196802.

(8) Zhang, C.; Johnson, A.; Hsu, C.-L.; Li, L.-J.; Shih, C.-K. *Nano Lett.* **2014**, *14*, 2443−2447.

(9) Zhao, Y.; Xu, K.; Pan, F.; Zhou, C.; Zhou, F.; Chai, Y. *Adv. Funct. Mater.* **2017**, *27*, 1603484.

(10) Allain, A.; Kang, J.; Banerjee, K.; Kis, A. *Nat. Mater.* **2015**, *14*, 1195−1205.

(11) Das, S.; Chen, H.-Y.; Penumatcha, A. V.; Appenzeller, J. *Nano Lett.* **2013**, *13*, 100−105.

(12) Kwon, J.; Lee, J.-Y.; Yu, Y.-J.; Lee, C.-H.; Cui, X.; Hone, J.; Lee, G.-H. *Nanoscale* **2017**, *9*, 6151−6157.

(13) Cui, X.; Lee, G.-H.; Kim, Y. D.; Arefe, G.; Huang, P. Y.; Lee, C.-H.; Chenet, D. A.; Zhang, X.; Wang, L.; Ye, F.; Pizzocchero, F.; Jessen, B. S.; Watanabe, K.; Taniguchi, T.; Muller, D. A.; Low, T.; Kim, P.; Hone, J. *Nat. Nanotechnol.* **2015**, *10*, 534−540.

(14) Yu, L.; Lee, Y.-H.; Ling, X.; Santos, E. J. G.; Shin, Y. C.; Lin, Y.; Dubey, M.; Kaxiras, E.; Kong, J.; Wang, H.; Palacios, T. *Nano Lett.* **2014**, *14*, 3055−3063.

(15) Pisoni, R.; Lee, Y.; Overweg, H.; Eich, M.; Simonet, P.; Watanabe, K.; Taniguchi, T.; Gorbachev, R.; Ihn, T.; Ensslin, K. 2017, arXiv preprint arXiv:1701. 08619.

(16) Chuang, H.-J.; Chamlagain, B.; Koehler, M.; Perera, M. M.; Yan, J.; Mandrus, D.; Tománek, D.; Zhou, Z. *Nano Lett.* **2016**, *16*, 1896−1902.

(17) Baugher, B. W. H.; Churchill, H. O. H.; Yang, Y.; Jarillo-Herrero, P. *Nano Lett.* **2013**, *13*, 4212−4216.

(18) Perera, M. M.; Lin, M.-W.; Chuang, H.-J.; Chamlagain, B. P.; Wang, C.; Tan, X.; Cheng, M. M.-C.; Tománek, D.; Zhou, Z. *ACS Nano* **2013**, *7*, 4449−4458.

(19) Chuang, H.-J.; Tan, X.; Ghimire, N. J.; Perera, M. M.; Chamlagain, B.; Cheng, M. M.-C.; Yan, J.; Mandrus, D.; Tománek, D.; Zhou, Z. *Nano Lett.* **2014**, *14*, 3594−3601.

(20) Kappera, R.; Voiry, D.; Yalcin, S. E.; Branch, B.; Gupta, G.; Mohite, A. D.; Chhowalla, M. *Nat. Mater.* **2014**, *13*, 1128−1134.

(21) Xu, S.; Wu, Z.; Lu, H.; Han, Y.; Long, G.; Chen, X.; Han, T.; Ye, W.; Wu, Y.; Lin, J.; Shen, J.; Cai, Y.; He, Y.; Zhang, F.; Lortz, R.; Cheng, C.; Wang, N. *2D Mater.* **2016**, *3*, 021007.

(22) Wu, Z.; Xu, S.; Lu, H.; Khamoshi, A.; Liu, G.-B.; Han, T.; Wu, Y.; Lin, J.; Long, G.; He, Y.; Cai, Y.; Yao, Y.; Zhang, F.; Wang, N. *Nat. Commun.* **2016**, *7*, 12955.

(23) Chen, J.-R.; Odenthal, P. M.; Swartz, A. G.; Floyd, G. C.; Wen, H.; Luo, K. Y.; Kawakami, R. K. *Nano Lett.* **2013**, *13*, 3106−3110.

(24) Dankert, A.; Langouche, L.; Kamalakar, M. V.; Dash, S. P. *ACS Nano* **2014**, *8*, 476−482.

(25) Wang, J.; Yao, Q.; Huang, C.-W.; Zou, X.; Liao, L.; Chen, S.; Fan, Z.; Zhang, K.; Wu, W.; Xiao, X.; et al. *Adv. Mater.* **2016**, *28*, 8302−8308.

(26) Fallahazad, B.; Movva, H. C. P.; Kim, K.; Larentis, S.; Taniguchi, T.; Watanabe, K.; Banerjee, S. K.; Tutuc, E. *Phys. Rev. Lett.* **2016**.

(27) Sui, M.; Chen, G.; Ma, L.; Shan, W.-Y.; Tian, D.; Watanabe, K.; Taniguchi, T.; Jin, X.; Yao, W.; Xiao, D.; Zhang, Y. *Nat. Phys.* **2015**, *11*, 1027−1031.

(28) Chen, H.; Wen, X.; Zhang, J.; Wu, T.; Gong, Y.; Zhang, X.; Yuan, J.; Yi, C.; Lou, J.; Ajayan, P. M.; Zhuang, W.; Zhang, G.; Zheng, J. *Nat. Commun.* **2016**, *7*, 12512.

(29) Fogler, M. M.; Butov, L. V.; Novoselov, K. S. *Nat. Commun.* **2014**, *5*, 4555.

(30) Farmanbar, M.; Brocks, G. *Phys. Rev. B: Condens. Matter Mater. Phys.* **2015**, *91*, 161304.

(31) Farmanbar, M.; Brocks, G. *Adv. Electron. Mater.* **2016**, *2*, 1500405.

(32) Wang, L.; Meric, I.; Huang, P. Y.; Gao, Q.; Gao, Y.; Tran, H.; Taniguchi, T.; Watanabe, K.; Campos, L. M.; Muller, D. A.; Guo, J.; Kim, P.; Hone, J.; Shepard, K. L.; Dean, C. R. *Science* **2013**, *342*, 614−617.

(33) Brugger, T. *Graphene and Hexagonal Boron Nitride on Transition Metals and Their Application*; Univ. Zürich, 2010.

(34) Haynes, W. M. *CRC Handbook of Chemistry and Physics*, 95th ed.; CRC Press, 2014.

(35) Kaushik, N.; Karmakar, D.; Nipane, A.; Karande, S.; Lodha, S. *ACS Appl. Mater. Interfaces* **2016**, *8*, 256−263.

(36) Lee, S.; Tang, A.; Aloni, S.; Wong, H.-S. P. *Nano Lett.* **2016**, *16*, 276−281.

(37) Kaushik, N.; Nipane, A.; Basheer, F.; Dubey, S.; Grover, S.; Deshmukh, M. M.; Lodha, S. *Appl. Phys. Lett.* **2014**, *105*, 113505.

(38) Britnell, L.; Gorbachev, R. V.; Jalil, R.; Belle, B. D.; Schedin, F.; Katsnelson, M. I.; Eaves, L.; Morozov, S. V.; Mayorov, A. S.; Peres, N. M. R.; Neto, A. H. C.; Leist, J.; Geim, A. K.; Ponomarenko, L. A.; Novoselov, K. S. *Nano Lett.* **2012**, *12*, 1707−1710.

(39) Lee, G.-H.; Yu, Y.-J.; Lee, C.; Dean, C.; Shepard, K. L.; Kim, P.; Hone, J. *Appl. Phys. Lett.* **2011**, *99*, 243114.

(40) Britnell, L.; Gorbachev, R. V.; Jalil, R.; Belle, B. D.; Schedin, F.; Mishchenko, A.; Georgiou, T.; Katsnelson, M. I.; Eaves, L.; Morozov, S. V.; Peres, N. M. R.; Leist, J.; Geim, A. K.; Novoselov, K. S.; Ponomarenko, L. A. *Science* **2012**, *335*, 947−950.

(41) Radisavljevic, B.; Kis, A. *Nat. Mater.* **2013**, *12*, 815−820.

(42) Joo, M.-K.; Moon, B. H.; Ji, H.; Han, G. H.; Kim, H.; Lee, G.; Lim, S. C.; Suh, D.; Lee, Y. H. *Nano Lett.* **2016**, *16*, 6383−6389.

(43) Kretinin, A. V.; Cao, Y.; Tu, J. S.; Yu, G. L.; Jalil, R.; Novoselov, K. S.; Haigh, S. J.; Gholinia, A.; Mishchenko, A.; Lozada, M.; Georgiou, T.; Woods, C. R.; Withers, F.; Blake, P.; Eda, G.; Wirsig, A.; Hucho, C.; Watanabe, K.; Taniguchi, T.; Geim, A. K.; Gorbachev, R. V. *Nano Lett.* **2014**, *14*, 3270−3276.

(44) Srivastava, A.; Sidler, M.; Allain, A. V.; Lembke, D. S.; Kis, A.; Imamoğlu, A. *Nat. Phys.* **2015**, *11*, 141−147.

(45) Li, Y.; Ludwig, J.; Low, T.; Chernikov, A.; Cui, X.; Arefe, G.; Kim, Y. D.; van der Zande, A. M.; Rigosi, A.; Hill, H. M.; Kim, S. H.; Hone, J.; Li, Z.; Smirnov, D.; Heinz, T. F. *Phys. Rev. Lett.* **2014**, *113*, 266804.

(46) English, C. D.; Shine, G.; Dorgan, V. E.; Saraswat, K. C.; Pop, E. *Nano Lett.* **2016**, *16*, 3824−3830.

DOI: 10.1021/acs.nanolett.7b01536
Nano Lett. 2017, 17, 4781−4786